

Signal Formation in THGEM-like Detectors

Purba Bhattacharya^{a*1}, Luca Moleri^b, Shikma Bressler^a

^a *Department of Particle Physics and AstroPhysics, Weizmann Institute of Science, Herzl St. 234, Rehovot - 7610001, Israel*

^b *Department of Physics, Technion - Israel Institute of Technology, Haifa - 3200003, Israel*

Abstract

Numerical simulations were used to study signal formation in a Thick Gaseous Electron Multiplier (THGEM) and in THGEM -based Thick-WELL (THWELL) and Resistive-Plate WELL (RPWELL) detectors. The signal shapes were simulated in mixtures of Argon and Neon with 5% Methane under irradiation with soft x-rays and muons. Anode-induced raw signals were convoluted with the response functions of charge-sensitive and current-sensitive pre-amplifiers. The simulation toolkit was validated by the good agreement reached between the simulated and measured response, with different pre-amplifiers. It indicates that our simulations framework provides valid insight into the inherent complex dynamical processes of the various detectors.

Keywords: THGEM-based Detectors, Anode-induced Signals, Charge and Current-Sensitive Pre-Amplifiers, Convoluted Signals

***Corresponding Author:** Purba Bhattacharya

E-mail: purba.bhattacharya85@gmail.com

1 Introduction

Signals resulting from radiation-induced charges in gaseous radiation detectors, drifting under electric field and multiplied in a gas-avalanche mode - provide information on the deposited energy and position of the interacting event. The current induced on a specific electrode by a drifting charge can be calculated from the Shockley-Ramo Theorem [1, 2]. The induced charge in the detector is constant along its drift path, under an applied electric field. The shape of the currents induced by drifting electrons and ions, depends on the detector type and geometry, on the electric-field distribution and on the charge mobility in a given gas [3–6].

Charge-sensitive preamplifiers are often used to provide an output voltage pulse of amplitude proportional to the integral of the varying-in-time input current pulse. The output pulse can be obtained by convoluting the input current with the pre-amplifier’s response (transfer function). For more details see [4, 5].

In this work, we have used Garfield [7, 8] in combination with neBEM [9, 10], Magboltz [11, 12] and Heed [13, 14] software packages for evaluating the signal formation in some Thick Gaseous Electron Multiplier (THGEM)-like detectors [15, 16]: standard THGEM, Thick WELL (THWELL) [17] and Resistive-Plate WELL (RPWELL) [18]. Their schematic descriptions are shown in Figure 1. They share similar geometrical and material features.

A comprehensive comparison of their simulated signal shapes is presented in this work and compared to experimental results. Note that similar framework was used in the past for simulating the signal shapes in Micromegas [19] and RPC [20] detectors. In the process of evaluating the signal shapes from the THGEM-based detectors, we have also convoluted the raw signals with the transfer functions of the different pre-amplifiers employed to reproduce the experimental conditions.

The detector geometries are discussed in section 2. The simulation method is detailed in section 3. The experimental setup is described in section 4, followed by the results in section 5 and a discussion in section 6.

2 THGEM-based Detectors

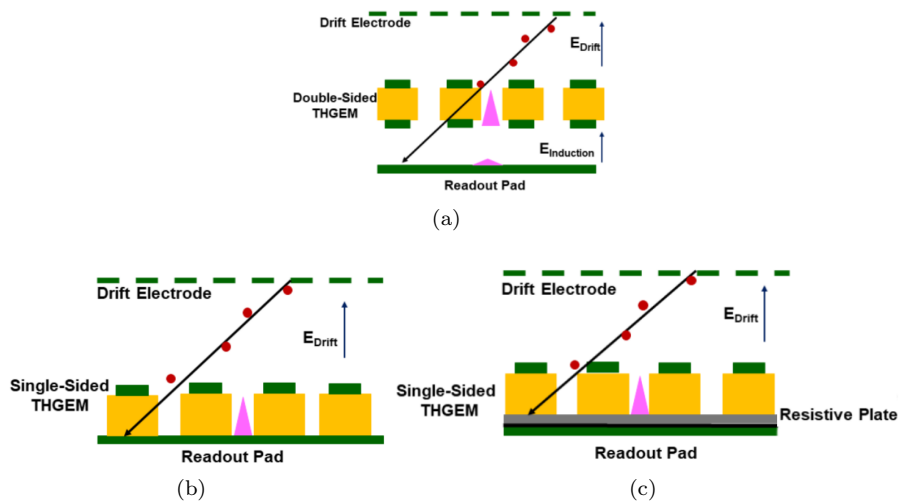


Figure 1: A schematic view of the (a) double-sided THGEM with an induction gap, (b) THWELL and (c) RPWELL detectors..

The THGEM [15, 16, 21, 22] is a simple and robust detector suitable for applications requiring large-area detection surfaces with moderate spatial resolution ($\sim 0.2 - 0.3$ mm RMS). In its original configuration, a THGEM electrode is made of a sub – mm thick double-sided printed-circuit board (Cu-clad on both surfaces) having mechanically-drilled holes typically ~ 0.5 mm in diameter with chemically etched rims, patterned over the surface with ~ 1 mm pitch (Fig. 1a). Single-sided THGEM electrodes (copper-clad

on its top side only) are used for WELL configurations, in which a readout anode is coupled directly (THWELL, Fig. 1b) or via resistive material (Resistive WELL [17] and the RPWELL (Fig. 1c)) to the multiplier's bottom surface. The resistive coating of the anode of its coupling through a resistive plate aim at quenching occasional discharges. A stable operation of RPWELL detectors in muon- and hadron-beams, was demonstrated in neon- and argon-based gas mixtures [23–26].

In its standard configuration (Figure 1(a)), the THGEM electrode is preceded by a conversion and drift gap. Radiation-induced ionization electrons drift into the THGEM holes, where multiplication occurs under a high electric field. The resulting avalanche electrons are extracted into a few-mm wide induction gap and drift towards the readout anode, inducing a signal. As long as the field strength in the induction gap is below the multiplication threshold, the induced signal (measured on the readout anode) is characterized by a fast rise time (of a few nsec). The anode is sensitive essentially only to the motion of avalanche electrons along the induction gap; the ion movement occurs within the THGEM hole, far from the anode, and has a negligible effect on the pulse shape [27]. In the THWELL (Figure 1(b)), higher gains could be obtained at a given applied voltage across the THGEM electrode, due to the larger electric field within the closed holes. The signal induced on the THWELL anode plate is characterized by a fast rise (avalanche electrons) followed by a slow avalanche-ion component [27]. In the RPWELL, the electrode is coupled to a thin plate of high bulk resistivity ($\sim 10^9 - 10^{12} \Omega\text{cm}$), with the patterned readout anode placed behind [18]. Despite of the additional Resistive Plate (RP), the pulse shape on the anode is similar to that of the THWELL [18,27].

Table 1: The investigated-detector configurations and operation parameters.

Detector	Thickness	Gas Mixture	Voltage [V]
THGEM	0.8 mm	Ar/(5%)CH ₄	2000
THGEM	0.6 mm	Ar/(5%)CH ₄	1600
THWELL	0.8 mm	Ar/(5%)CH ₄	1700
THWELL	0.4 mm	Ar/(5%)CH ₄	1200
RPWELL	0.8 mm	Ar/(5%)CH ₄	1750
RPWELL	0.8 mm	Ne/(5%)CH ₄	975
RPWELL	0.4 mm	Ar/(5%)CH ₄	1250
RPWELL	0.4 mm	Ne/(5%)CH ₄	850

In the present work, three types of detectors were investigated: 1) 0.6 and 0.8 mm thick double-sided single THGEM detectors (with induction gap), 2) 0.4 and 0.8 mm thick THWELL detectors and 3) 0.4 and 0.8 mm thick RPWELL detectors. In the RPWELL, the resistive plate (RP) consisted of a 0.4 mm thick Semitron ESD225 static dissipative acetal material with a bulk resistivity of $\sim 10^9 \Omega\text{cm}$ [28]. In all of the cases, the hole diameter and pitch are 0.5 mm and 1 mm, respectively. Avalanche electrons in the RPWELL holes, traversing the RP are evacuated to ground through the RP bottom surface - coated with a thin layer of graphite (surface resistivity $\sim 3 \text{ M}\Omega/\text{sq}$) [26]. The geometrical and voltage configurations of the investigated detectors are summarized in Table 1. The drift gap in all configurations was kept at 5 mm, with spacers between the cathode mesh and the multiplier's top electrode; the drift field in all experiments was 0.5 kV/cm. The THGEM detector was operated with a 2 mm wide induction gap (Figure 1(a)), under an induction field of 2 kV/cm (below charge multiplication onset).

3 Numerical Model

Garfield simulation framework [7] has been used in the present work. The 3D electrostatic field simulations have been carried out with the neBEM (nearly exact Boundary Element Method) toolkit [9]. HEED [13] has been used for primary-ionization calculations and Magboltz [11] - for computing drift, diffusion as well as Townsend and attachment coefficients.

The design parameters of the THGEM-based detectors considered in the numerical simulations are those described in section 2. The RP of the RPWELL detector was considered to be a dielectric - transparent to the signals induced on the anode [29]. The basic electrode's cell structure has been

repeated along both X- and Y-axes, to represent a real detector. The field configurations of the different detectors have been simulated using the voltage settings mentioned in Table 1.

Primary-electron clusters were generated for 5.9 keV photons and relativistic muons interacting with the detector medium; the latter being distributed along a track portion depositing energy within the drift gap (Fig. 2). The primary-electrons' drift process towards the THGEM electrode was simulated using the Microscopic tracking routine [7]. In this procedure, a typical drift path proceeds through millions of collisions, each being classified as elastic or inelastic (including excitation, ionization, attachment etc.). The electrons are focused into the holes by the drift- and the hole's dipole fields, inducing avalanches within the holes. In this process, an electron starting from a given point is subject to collisions with gas molecules; at each step, a number of secondary electrons are produced according to the local Townsend and attachment coefficients; the newly produced electrons are traced like the initial ones. In parallel, the ions' drift lines are traced.

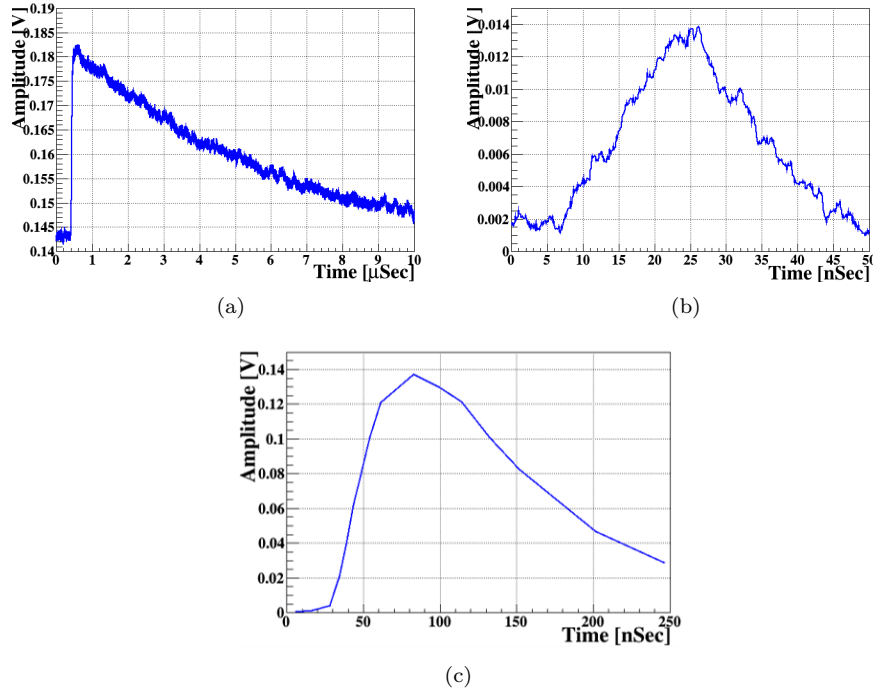


Figure 2: The measured response functions to a square pulse (with 200 μ sec width, 50 mV amplitude), injected through an ORTEC pulse generator charge terminator (2 pF, 100 Ω), of (a) charge-sensitive Canberra 2006 and (b) custom -made, fast current pre-amplifier. (c) The response function of the APV25 chip as reported in [30]

In a medium with perfect conductors and insulators, the current induced by a moving charge q onto an electrode can be calculated by means of the Shockley-Ramo theorem [2,3]. The current \mathcal{I} that flows into one particular electrode i under the influence of a charge q moving with velocity v can be calculated using the following equation:

$$\mathcal{I} = -q \frac{\vec{v} \times \vec{E}_w}{V} \quad (1)$$

Here E_w is the field created by raising this electrode to a potential V and grounding all other electrodes, in the absence of charge.

The total charge Q induced on the electrode is given by

$$Q = \int_0^{\Delta t} i(t) dt = q \Delta V_w \quad (2)$$

89 ΔV_w is the weighting potential difference across which the charge has drifted.

90 We used the Shockley-Ramo theorem to calculate the induced current on a uniform readout anode.
 91 The current pulse was then convoluted with the readout electronics response function. The output voltage
 92 from the preamplifier is then:

$$V(t) = i(t) \otimes h(t) \quad (3)$$

93 The response functions of a charge sensitive and a fast pre-amplifier (used here) are shown in Figure
 94 2. The response function of the APV25 chip [30] (Figure 2(c)) was taken from [30].

95 4 Experimental setup

96 The experimental setup in lab, is shown in Figure 3. The investigated detectors were placed in an
 97 aluminum vessel flushed with Ar/5%CH₄ and Ne/5%CH₄ at a flow of 25 sccm (standard cubic centimeters
 98 per minute) at atmospheric pressure. The detectors were investigated at the Laboratory with ⁵⁵Fe-source
 99 5.9 KeV x-rays and cosmic muons; complementary measurements with an RPWELL detector were carried
 100 out at CERN-SPS with 150 GeV muons.

101 The drift electrode and the multipliers top electrode (and bottom electrode in the case of the THGEM)
 102 were polarized, through low-pass filters, by CAEN N1471H HV power supplies. In all configurations, the
 103 anode was at ground potential. In the laboratory studies, anode signals (in the THGEM configuration
 104 readout-anode signals after the induction gap) were recorded through a charge-sensitive pre-amplifier
 105 (Canberra 2006; decay-time of 50 μ sec) and a custom-made fast current pre-amplifier having shaping
 106 time of ~ 25 nsec. The preamplifier signals were processed by an Agilent Technologies InfiniVision
 107 DSO-X 3034A digital oscilloscope. In all detector configurations, the voltage values across the multiplier
 108 (Table 1) were adjusted to keep similar gas gains of ~ 4000 .

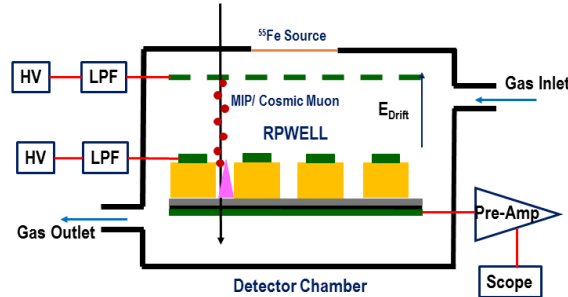


Figure 3: A schematic view of the experimental setup. The detectors (shown is a RPWELL), placed in a vessel under gas flow, are irradiated by an external radiation source or charged particles. Signals from the anode (in a THGEM, after an induction gap; see text) are recorded with the pre-amplifier and processed by a digital oscilloscope. The detector electrodes are polarized through low-pass filters by high voltage power supplies .

109 In the CERN-SPS (H2 RD51 Test Beam area) accelerator measurements, the signal shapes of a 0.8 mm
 110 thick RPWELL detector were studied in Ne/5%CH₄. The signal pulses were recorded by an APV25 fast
 111 current pre-amplifier chip [30] (shaping time of 75 nsec); they were further processed and digitized by an
 112 SRS readout system [31]. The latter has been frequently used to characterize the performance of MPGD
 113 detectors [32,33], including the THGEM and RPWELL ones [23,24].

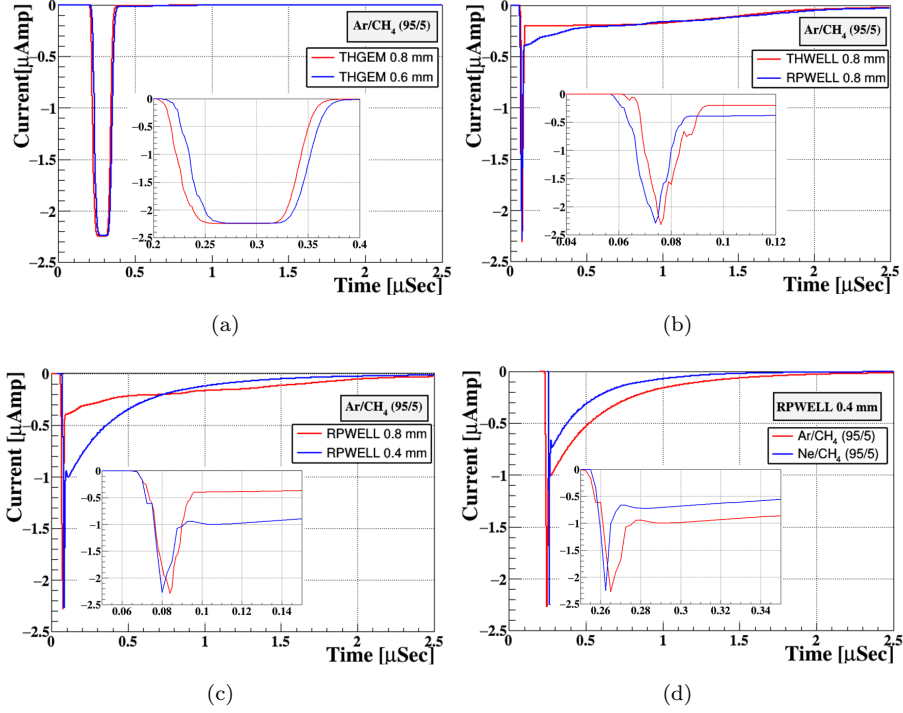


Figure 4: Simulated raw signals induced by 5.9 keV photons in (a) a THGEM with induction gap, (b) in 0.8 mm thick THWELL and RPWELL detectors, (c) in 0.8 and 0.4 mm thick RPWELL detectors in Ar/5%CH₄. (d) Signals in a 0.4 mm thick RPWELL detector in Ar/5%CH₄ and Ne/5%CH₄. The fast signals are shown in the inset. The time axis of the insets is also in μsec .

5 Results

5.1 Response to 5.9 keV photons

5.1.1 Simulated Raw Current Signals

Typical simulated 5.9 keV x-ray-induced raw current signals in the THGEM detector (Figure 1(a)) are shown in Figure 4(a) for 0.6 and 0.8 mm thick electrodes. The induced currents are due to the movement of avalanche electrons extracted from the hole, along the induction gap - towards the readout-anode plate. In this configuration, there are no ions drifting along the induction gap (no slow ion component). The signal length dictated by electron drift along the 2 mm induction gap is ~ 120 nsec; the 0.2 mm thickness variation does not affect this time by more than $\sim 1\%$.

The raw current signals of the THWELL and RPWELL detectors are shown in Figure 4(b); the fast pulse is due to the avalanche electrons, whereas the long tail is the result of the ions' drift away from the avalanche head. The RPWELL current signals are peaked similarly to that of the THWELL; however, the ion-component shape is different in both detectors. Due to the presence of the resistive layer (Figure 1(c)), the weighting field in the RPWELL is different from that of the THWELL detector. But, in both cases, the ion tail reaches zero value within $\sim 2 \mu\text{sec}$. The raw current signal of RPWELL detectors having thickness of 0.8 mm and 0.4 mm are shown in Figure 4(c). The rise-time for the 0.8 mm thick electrode is ~ 15 nsec, whereas for 0.4 mm thick one it is ~ 11 nsec. Throughout this paper, the time required for the response to rise from 10% to 90% of its maximum value is defined as the rise time of the signal. The decay time of the ion tail for the thicker electrode is $\sim 1.7 \mu\text{sec}$ in comparison to $\sim 0.8 \mu\text{sec}$ for the thinner one, consistent with the shorter ion drift time to the top electrode. A comparison of the raw signals of a 0.4 mm thick RPWELL detector in Ar/5%CH₄ and Ar/5%CH₄ is shown in Figure 4(d). The ion tail in the Ne-mixture decays faster than that in the Ar-mixture; it is consistent with the faster ion velocity in the former.

5.1.2 Charge-sensitive Pre-amplifier response: Measurements and Simulations

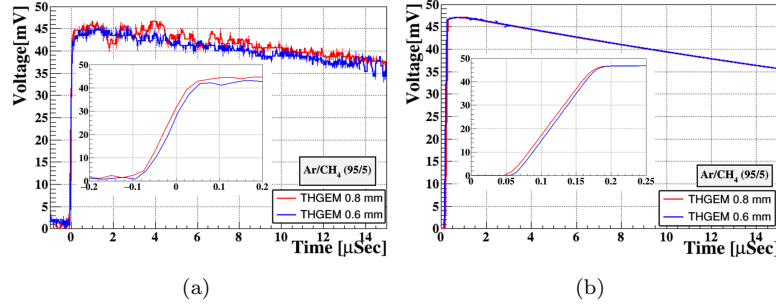


Figure 5: Measured and simulated charge-pre-amplifier pulses, induced by 5.9 keV photons in THGEM (a) measurement, (b) simulation. Electrode thickness: 0.8 mm and 0.6 mm; gas: Ar/5%CH₄. The pulse rise-times of the THGEM are shown in the inset. The time axis of the insets is also in μsec .

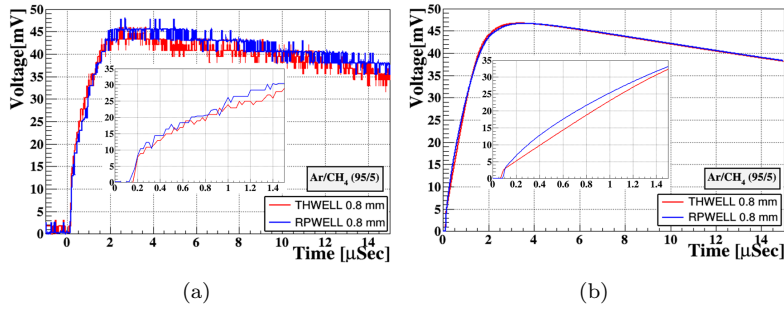


Figure 6: A comparison of the (a) measured and (b) simulated charge-signal shapes in 0.8 mm thick THWELL and RPWELL detectors, operated in Ar/5%CH₄. The fast and slow components of the two detectors are shown in the inset. The time axis of the insets is also in μsec .

Charge-sensitive pre-amplifier signals measured on the anodes of the THGEM are shown in Figures 5(a). The rise-time of the THGEM pulse, reflecting the avalanche-electrons drift to the anode, is ~ 100 nsec. The respective simulated charge signal is shown in Figures 5(b). As discussed in Section 3, the raw current signals (Figure 4) are convoluted with the response function of the pre-amplifier. The decay time, determined by the decay constant of the pre-amplifier, is long, of the order of few tenths of μsec . A comparison of the measured and simulated charge-signal shapes of THWELL and RPWELL detectors are shown in Figure 6. There is no significant difference in the signal shapes. The RPWELL detectors pulses have ~ 1.9 and ~ 1.0 μsec rise for respective electrode thicknesses of 0.8 and 0.4 mm (longer ion drift time along the holes) as shown in Figure 7. In all the above cases, the simulated data are in good agreement with the experimental data.

A comparison of the measured and simulated signal shapes of the 0.4 mm thick RPWELL detector in Ar/5%CH₄ and in Ne/5%CH₄ are shown in Figure 8. The simulated ion-component rise-time in the Ne mixture is faster than that in the Ar one, which is consistent with the fast ion mobility in Ne-based gas mixture. The experimental signals (8(a)) are in good agreement with the simulated ones (8(b)).

5.1.3 Current Pre-amplifier response: Measurements and Simulations

The measured and simulated fast-current signals induced by x-rays in THGEM detector, recorded with the custom-made current-sensitive pre-amplifier are shown in Figure 9. Due to the pre-amplifier shaping time, the THGEM pulses have a rise-time of ~ 25 nsec and a width of ~ 100 nsec (electron drift time within the induction gap). A comparison of measured and simulated fast current-signal shapes, recorded with the custom-made current preamplifier, in 0.8 mm thick THWELL and RPWELL detectors are shown

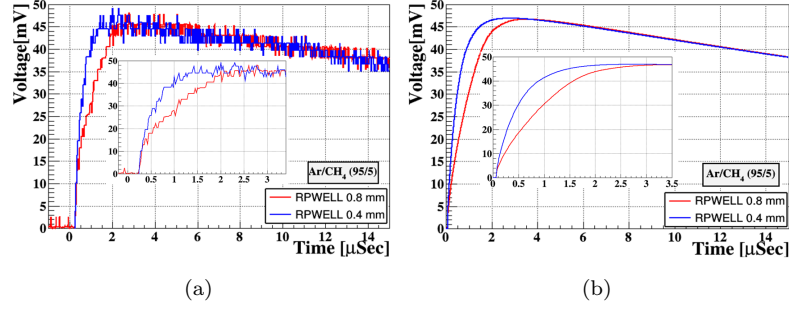


Figure 7: Measured and simulated charge-pre-amplifier pulses, induced by 5.9 keV photons in RPWELL (a) measurement, (b) simulation. Electrode thickness: 0.8 mm and 0.4 mm; gas: Ar/5%CH₄. The pulse rise-times of the RPWELL are shown in the inset. The time axis of the insets is also in μsec .

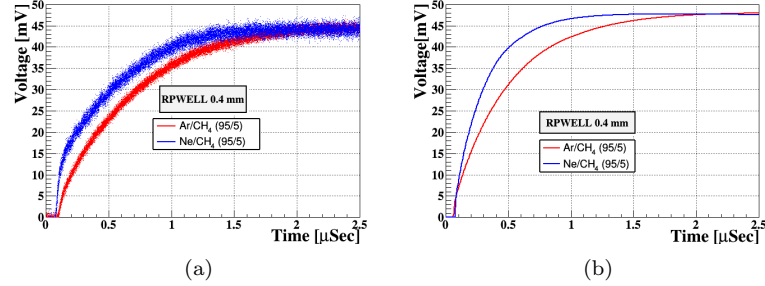


Figure 8: A comparison of the (a) measured and (b) simulated charge-signal shapes in a 0.4 mm thick RPWELL detector, operated in Ar/5%CH₄ and in Ne/5%CH₄

in Figure 10. The THWELL and RPWELL detectors pulses are narrower; they have a faster rise-time, of ~ 10 nsec. The current peak is followed by a long ion tail, more pronounced in the simulation than in the measurement. The electrode thickness does not affect the signals' rise time of RPWELL detectors as shown in Figure 11. The effect of the gas mixture on the signal shape in the RPWELL detector is shown in Figure 12.

5.2 Response to Cosmic Muons: Measurements and Simulations

While the soft x-ray photons induce local electron clusters in each interaction in the 5 mm drift gap, cosmic muons induce extended ionization charges along their tracks; a computed distribution of ionization clusters within the 5 mm gap is shown in Figure 13(a). The electron drift time from a cluster positioned close to a hole could be at the order of a few nsec; others, drifting to the hole from distant locations generate trains of signals during a few 100 nsec. Due to its long shaping time, a typical signal of a charge-sensitive pre-amplifier will consist of fast electron-component signals on top of the long ion-component. Signals from a current-sensitive pre-amplifier exhibit cluster-induced peaks as shown in Figure 13(b) (measured) and 13(c) (simulated).

5.3 Response to accelerated Muons: Measurements and Simulation

We implemented our numerical model to simulate the signal shape measured with the APV25 chip, having ~ 75 nsec shaping time. Operated in ambient Ne/5%CH₄ gas, the 0.8 mm thick RPWELL detector (of 10×10 cm²) has been investigated with 150 GeV muons (normal incidence) at CERN-SPS. The signal shapes varied from track to track, according to the number of primary clusters and their location within the 5 mm long drift gap. As an example, two measured signals are shown in Figures 14(a) and 14(b). In these measurements, we used a strip-patterned readout anode and the signal was induced on a few neighboring strips [34]. For simplicity, in the simulation we assumed a continuous-non-patterned anode.

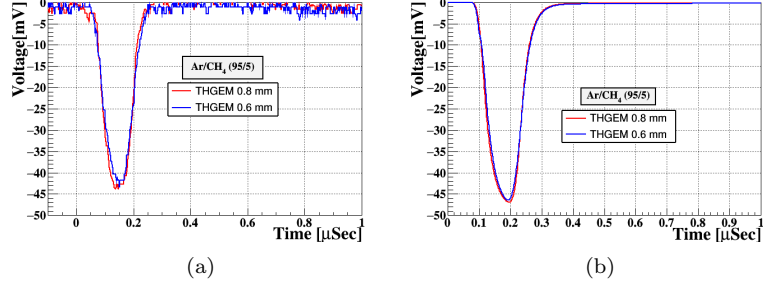


Figure 9: X-ray induced signals of 0.6 mm and 0.8 mm thick THGEM electrodes in Ar/5%CH₄ gas mixture measured with a current-sensitive pre-amplifier (custom-made): (a) measurement, (b) simulation

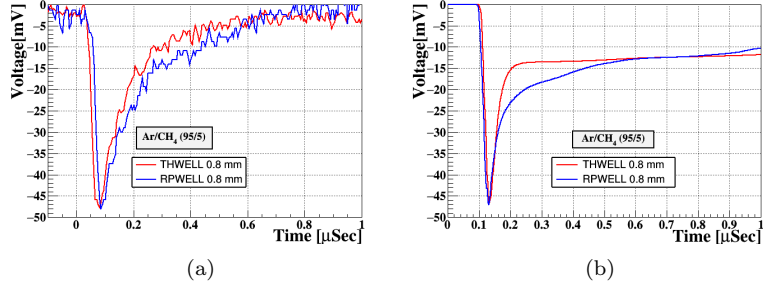


Figure 10: A comparison of the fast current signals in 0.8 mm thick THWELL and RPWELL detectors in Ar/5%CH₄ gas mixture measured from a custom-made current-sensitive pre-amplifier: (a) measurement, (b) simulation

A comparison of the shape of the signals induced on the central strip with the simulated one shows similar characteristics (Figure 14(c) and 14(d)).

6 Discussion

An evaluation of the signal formation in THGEM-like detectors is presented. The model-simulated signal shapes in THGEM (with induction gap), THWELL and RPWELL were validated by experimental results. The simulations were performed combining Garfield and neBEM packages. The signal shapes have been simulated in Ar/5%CH₄ and in Ne/5%CH₄ under irradiation with 5.9 keV x-ray photons, cosmic and relativistic muons. The raw signals were convoluted with the pre-amplifiers' response functions; the final signal forms were compared to that of measured signals in the three detector configurations investigated.

The soft-photon “point ionization” signals, measured by a fast preamplifier, differ from the “extended ionization” clustered muon-induced ones. The “clustering” effect is washed out using charge-sensitive pre-amplifiers of long shaping time; it is clearly observed with a fast current-pre-amplifier and with the APV25 chip having short shaping times. The difference between the signals in Ar- and Ne-based gas mixtures is reflected by the length of the ion-component tail (measured with a charge preamplifier); it is shorter in the Ne-based gas - due to higher ion mobility. The fast pre-amplifier, of ~ 50 nsec shaping time, integrates only 5 – 10% of the total charge. This effect should be taken into account when evaluating the detector gain. The variation of the detector thickness affects the slow ion's signal rise-time (with a charge-sensitive pre-amplifier), whereas the fast current (electrons mostly) signal does not reveal any significant change in the signal shape.

The effect of the RP is visible by comparing the ion component of the raw signal of the RPWELL to that of the THWELL. This affect is washed out when measuring with the charge sensitive pre-amplifier having long shaping time but is visible while using the fast pre-amplifier of short shaping time.

To summarise, rather good qualitative agreement was reached between the simulated and measured

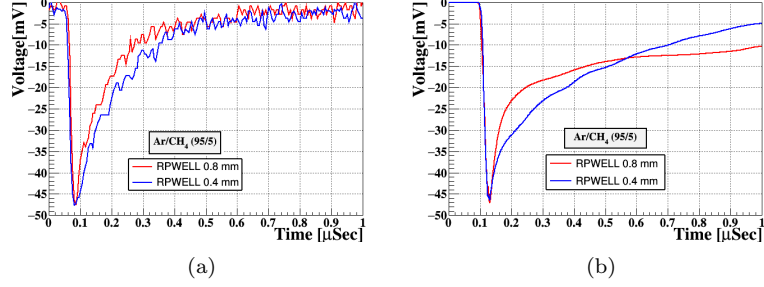


Figure 11: X-ray induced signals of 0.4 mm and 0.8 mm thick RPWELL detectors in Ar/5%CH₄ gas mixture measured with a current-sensitive pre-amplifier (custom-made): (a) measurement, (b) simulation.

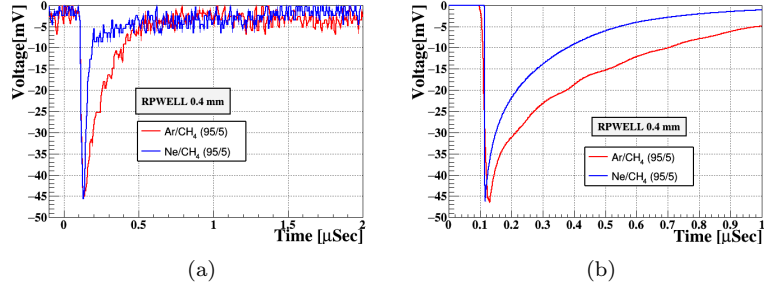


Figure 12: A comparison of the fast current signals in a 0.4 mm thick RPWELL detector in Ar/5%CH₄ and Ne/5%CH₄: (a) measurement, (b) simulation.

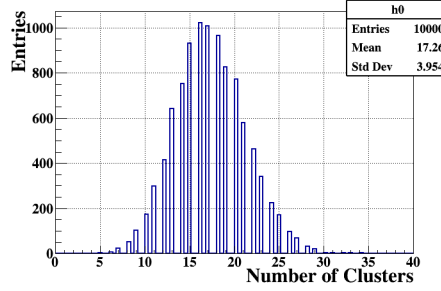
signal shapes, in all configurations investigated, under all irradiation conditions and gas mixtures. This confirms the success of the developed simulation tool - taking into account the important physics processes affecting the signal formation in these detectors as well as the response of the readout electronics. The model and the simulation kit provide a solid tool for conducting similar studies in other gas-avalanche detector configurations.

7 Acknowledgment

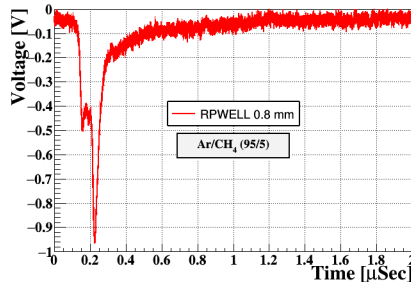
We thank Dr. R. Veenhof and Prof. S. Mukhopadhyay for their valuable suggestions and comments. This research was supported in part by the I-CORE Program of the Planning and Budgeting Committee, the Nella and Leon Benoziyo Center for High Energy Physics at the Weizmann Institute of Science and by Grant No 712482 from the Israeli Science Foundation (ISF).

References

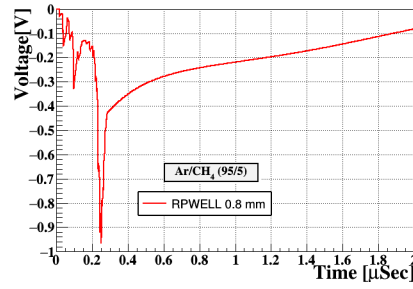
- [1] W. Shockley, Jour. Applied Phys. 9 (1938) 635.
- [2] S. Ramo, Proc. IRE, IEEE 27 (1939) 584.
- [3] W. Blum, W. Riegler, L. Rolandi, 2nd Edition (Springer, New York, NY) (2008).
- [4] G. F. Knoll, 3rd Edition, John Wiley & Sons.
- [5] F. Sauli, Cambridge Monographs on Particle Physics, Nucl. Phys. and Cosmology.
- [6] Kristen A. Recine, James B. R. Battat, Shawn Henderson, American Jour. Phys. 82 (2014) 322.
- [7] <http://cern.ch/garfield>.



(a)



(b)



(c)

Figure 13: RPWELL response to cosmic muons interacting in a normal direction to the detector surface, in Ar/5%CH₄. (a) A simulated Muon-induced Number-of-clusters distribution; (b) measured signal from a fast pre-amplifier; (c) simulated fast pre-amplifier signal.

- [8] R. Veenhof, Nucl. Instr. Meth., A 419 (1998) 726.
- [9] <http://cern.ch/neBEM>.
- [10] N. Majumdar, S. Mukhopadhyay, Jour. Instr. 2 (2007) P09006.
- [11] <http://cern.ch/magboltz>.
- [12] S.F. Biagi, Nucl. Instr. Meth. A 421 (1999) 234.
- [13] <http://cern.ch/heed>.
- [14] I.B. Smirnov, Nucl. Instr. Meth. A 554 (2005) 474.
- [15] R. Chechik, A. Breskin, C. Shalem, D. Mörmann, Nucl. Instr. Meth. A 535 (2004) 303.
- [16] A. Breskin et al., Nucl. Instr. Meth. A 598 (2009) 107.
- [17] S. Bressler, L. Arazi, L. Moleri, M. Pitt, A. Rubin, A. Breskin, Jour. Instr. 8 (2013) C12012.
- [18] A. Rubin, L. Arazi, S. Bressler, L. Moleri, M. Pitt, A. Breskin, Jour. Instr. 8 (2013) P11004.
- [19] P. Bhattacharya, S. Mukhopadhyay, N. Majumdar, S. Bhattacharya, Nucl. Instr. Meth. A 793 (2015) 41.
- [20] A. Jash, N. Majumdar, S. Mukhopadhyay, S. Saha, S. Chattopadhyay Jour. Instr. 11 (2016) C09014.
- [21] M. Alexeev et al., Jour. Instr. 5 (2010) P03009.
- [22] M. Alexeev et al., Nucl. Instr. Meth. A 639 (2011) 130.
- [23] S. Bressler et al., Jour. Instr. 11 (2016) P01005.

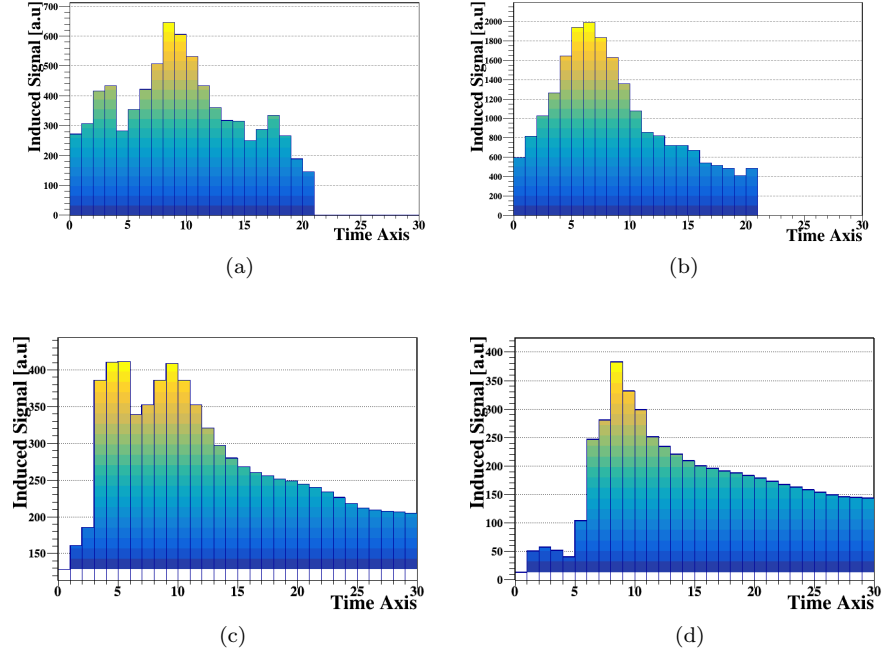


Figure 14: 150 GeV muon-induced signals within a 5 mm wide drift gap of an RPWELL detector operated in Ne/5%CH₄: (a) and (b) 2 examples of measured signals from an APV25 chip; (c) and (d) 2 examples of simulated signals, taking into account the response function of the APV25 chip.

- 238 [24] L. Moleri et al., Nucl. Instr. Meth. A 845 (2017) 262.
- 239 [25] S. Bressler et al., Jour. Instr. 8 (2013) P07017.
- 240 [26] L. Moleri et al., Jour. Instr. 11 (2016) P01093.
- 241 [27] L. Arazi, M. Pitt, S. Bressler, L. Moleri, A. Rubin, A. Breskin, Jour. Instr. 9 (2014) P04011.
- 242 [28] [https://www.quadrantplastics.com/na-en/products/engineering-plastics/advanced-325-425-](https://www.quadrantplastics.com/na-en/products/engineering-plastics/advanced-325-425-f/semitron-R-semiconductor-grade-products)
- 243 [f/semitron-R-semiconductor-grade-products](https://www.quadrantplastics.com/na-en/products/engineering-plastics/advanced-325-425-f/semitron-R-semiconductor-grade-products)
- 244 [29] W. Riegler, Nucl. Instr. Meth. A 491 (2002) 258.
- 245 [30] M. J. French et al., Nucl. Instr. Meth. A 466 (2001) 359.
- 246 [31] S. Martoiu, H. Muller, A. Tarazona, J. Toledo, Jour. Instr. 8 (2013) C03015.
- 247 [32] K. Gnanvo et al., IEEE Nucl. Sci. Symp. Conf. Rec. (2010) 552.
- 248 [33] V. Álvarez et al., Jour. Instr. 7 (2012) T06001.
- 249 [34] L. Moleri, P. Bhattacharya, A. E. C. Coimbra, A. Breskin, S. Bressler, Jour. Instr. 12 (2017) P10017.